Appendix file for

Loss of TDP-43 oligomerization or RNA binding elicits distinct aggregation patterns

Manuela Pérez-Berlanga, Vera I. Wiersma, Aurélie Zbinden, Laura De Vos, Ulrich Wagner, Chiara Foglieni, Izaskun Mallona, Katharina M. Betz, Antoine Cléry, Julien Weber, Zhongning Guo, Ruben Rigort, Pierre de Rossi, Ruchi Manglunia, Elena Tantardini, Sonu Sahadevan, Oliver Stach, Marian Hruska-Plochan, Frederic H.-T. Allain, Paolo Paganetti, Magdalini Polymenidou*

*Corresponding author. Email: magdalini.polymenidou@uzh.ch

Table of Contents:

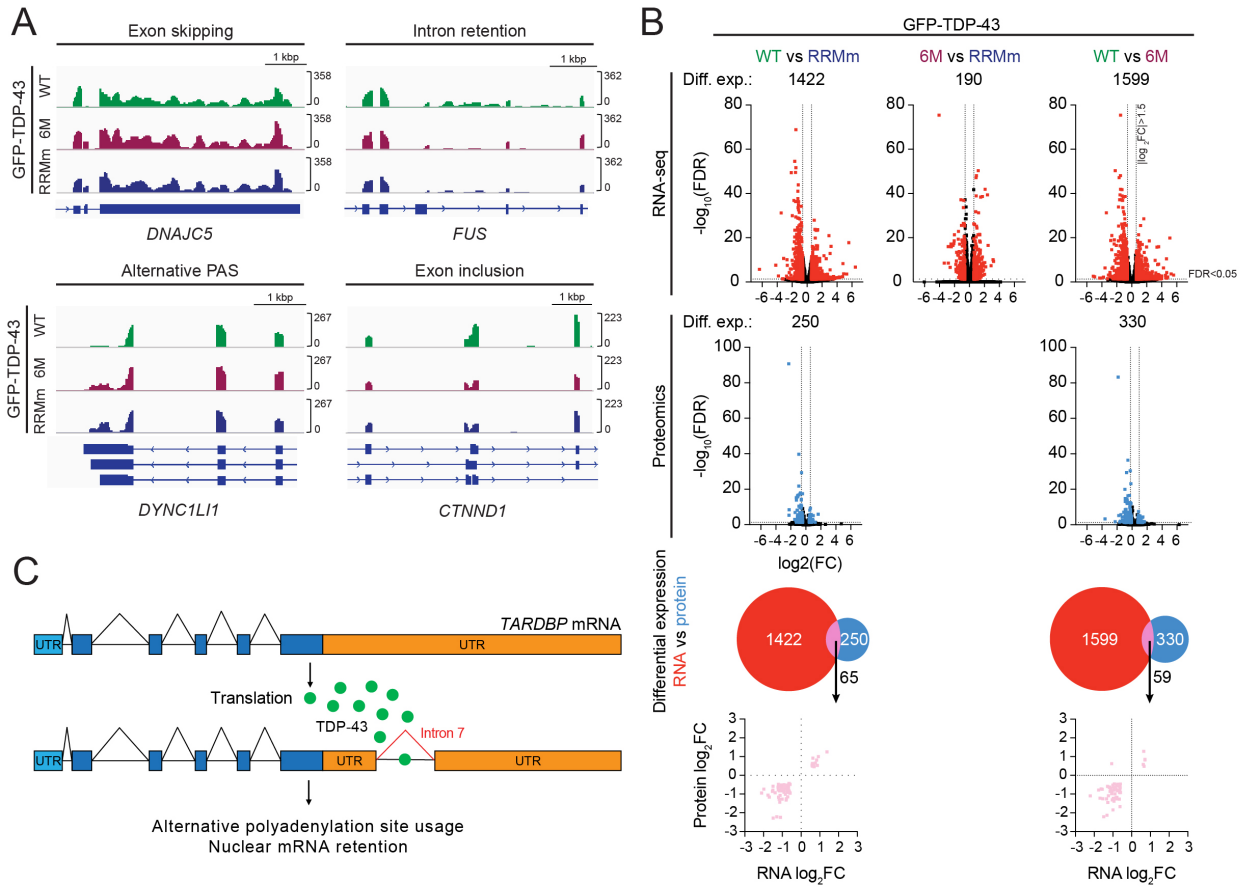
A
Exon skipping
Intron retention
Alternative PAS
Exon inclusion
GFP-TDP-43
WT
6M
RRMm
1 kbp
DNAJC5
FUS
DYNC1LI1
CTNND1
B
GFP-TDP-43
WT vs RRMm
6M vs RRMm
WT vs 6M
Diff. exp.:
1422
190
1599
250
330
RNA-seq
Proteomics
-log10(FDR)
log2(FC)
FDR<0.05
Differential expression
RNA vs protein
1422
250
65
1599
330
59
Protein log2FC
RNA log2FC
C
TARDBP mRNA
UTR
Translation
TDP-43
Intron 7
Alternative polyadenylation site usage
Nuclear mRNA retention
D
GFP-TDP-43 WT
DOX
siControl
siGFP
GFP
endTDP-43
SOD1
E
TDP-43/SOD1 levels (%)
****
F
GFP-TDP-43 mutNLS
WT
6M
RRMm
6M&RRMm
DOX
GFP
GAPDH
TDP-43
SOD1
G
Nucleus/cytoplasm
(mean GFP fluorescence)
GFP-TDP-43 mutNLS
H
GFP-TDP-43 mutNLS
GFP
G3BP
GFP intensity
I
GFP-TDP-43 mutNLS + 0.5 mM sodium arsenite
Merge
J
TDP-43+ SGs (%)
GFP-TDP-43 mutNLS

Appendix Figure S1. Functional TDP-43 oligomerization occurs in both the nucleus and the cytoplasm. (A) Representation of the RNA sequencing (RNA-seq) reads of examples of TDP-43-mediated alternative splicing events in the isogenic cell lines upon expression of the GFP-TDP-43 variants for 48 h (related to figure 6A). PAS: polyadenylation signal. **(B)** Volcano plots showing gene (top) and protein (bottom) expression changes (diff. exp.) upon expression of GFP-TDP-43 variants for 48 h. **(C)** Schematic representation of the mechanism of TDP-43 autoregulation **(Avendaño-Vázquez *et al*, 2012)**. **(D)** Western blot analysis depicting that autoregulation of endogenous TDP-43 (endTDP-43) takes place at lower WT GFP-TDP-43 levels. WT GFP-TDP-43 expression was induced with doxycycline (DOX) and simultaneously knocked down with an siRNA against GFP for 48 h. **(E)** Quantification of the endTDP-43 signal from D. N=3 independent experiments. Repeated measures one-way ANOVA with Greenhouse-Geisser correction and Tukey's multiple comparisons post hoc test. **(F)** Western blot analysis of the generated isogenic HEK293 cell lines expressing the GFP-TDP-43 mutNLS variants after protein expression for 48 h showing the tightness of the doxycycline (DOX)-modulated expression system in each line. **(G)** Quantification of nucleocytoplasmic levels of TDP-43 in immunocytochemistry images shown in H. N=3 independent experiments. One-way ANOVA with Tukey's multiple comparisons post hoc test. **(H)** Representative images of widefield fluorescence microscopy of the isogenic HEK293 cell lines expressing the GFP-TDP-43 mutNLS variants and stained for the cytoplasmic protein G3BP. GFP brightness is adjusted to the maximum values in each condition for optimal visualization of GFP-TDP-43 localization. Original intensity values are represented in the lower column using grayscale. Scale bar: 20 μm. **(I)** Representative confocal microscopy images of the isogenic HEK293 cell lines expressing the GFP-TDP-43 mutNLS variants for 3 hours followed by treatment with sodium arsenite for 45 minutes to induce SG formation. Note that arsenite treatment induced the formation of (mutant) GFP-TDP-43 mutNLS inclusions that did not overlap with the SG marker G3BP in all lines. Scale bar: 10 μm. **(J)** Quantification of the percentage of SGs showing GFP-TDP-43 incorporation per cell in the conditions described in I. N=143-183 cells. Kruskal-Wallis test with Dunn's multiple comparisons post hoc test. * $p<0.05$, ** $p<0.01$, *** $p<0.001$, **** $p<0.0001$. Graph bars represent mean ± SD and violin plots show mean and quartiles.

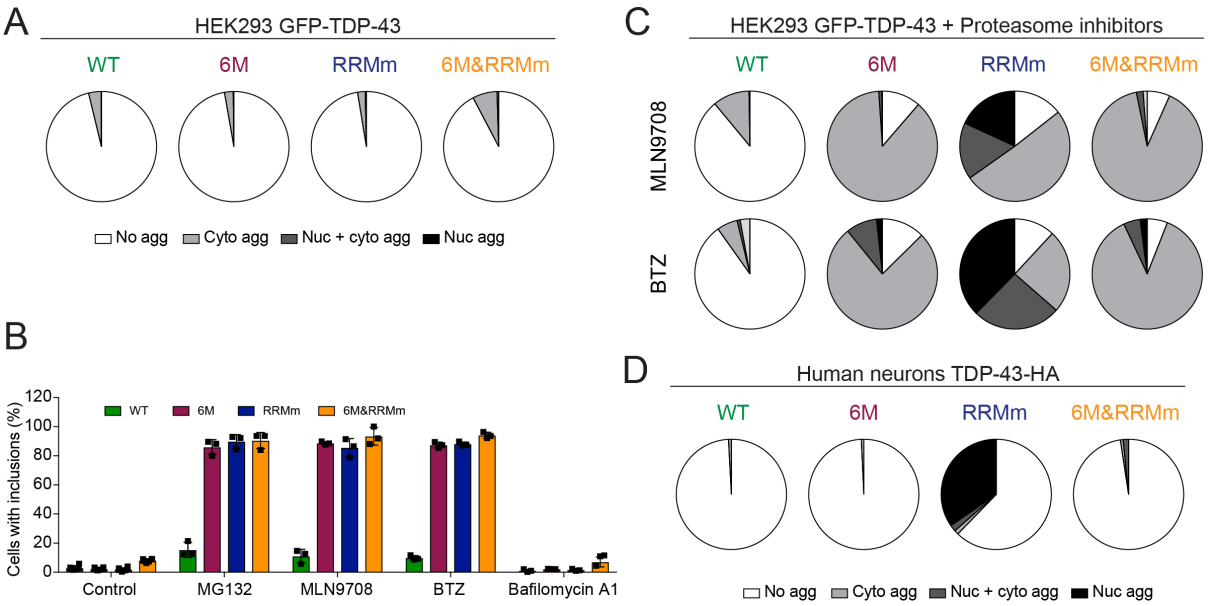

Appendix Figure S2. TDP-43 selectively aggregates upon proteasomal inhibition. (A) Quantification of the localization of the GFP-TDP-43 inclusions observed upon mock treatment with DMSO for the different GFP-TDP-43 variants in the isogenic HEK lines. Represented values are averages from N=3 replicates, with N=432-1166 cells quantified per condition and replicate. Agg: aggregates, Cyto: cytoplasmic, Nuc: nuclear. **(B)** Quantification of the number of cells harboring GFP-TDP-43 aggregates upon proteasome inhibition (MG132, MLN9708, BTZ) or autophagy disruption (bafilomycin A1) with the indicated compounds for 24 h. Represented values are averages from N=3 replicates, with N=28-1166 cells quantified per condition and replicate. **(C)** Quantification of the localization of GFP-TDP-43 inclusions induced by MLN9708 and bortezomib (BTZ) treatment for the different GFP-TDP-43 variants in the isogenic HEK lines. Represented values are averages from N=3 replicates, with N=28-359 cells quantified per condition and replicate. **(D)** Quantification of TDP-43-HA inclusions and their localization in human neurons upon mock treatment with DMSO. Represented values correspond to the quantification of N=118-159 cells from two independent experiments. Agg: aggregates, Cyto: cytoplasmic, Nuc: nuclear.

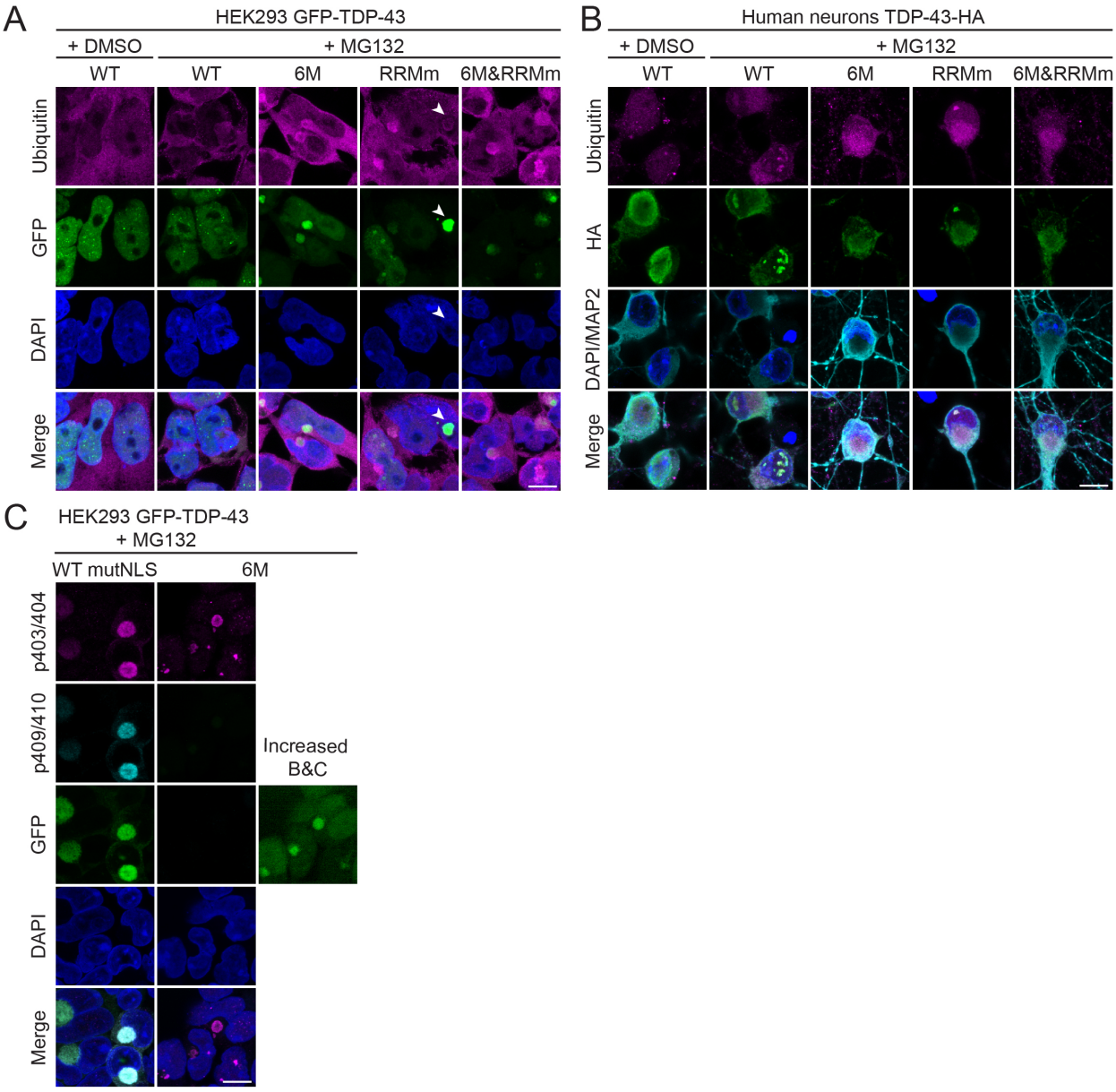

Appendix Figure S3. MG132-induced TDP-43 inclusions are ubiquitinated and variably phosphorylated. (A) Representative maximum intensity Z-projections from confocal fluorescence imaging (thickness of 4 µm, in steps of 1 µm) of the same experimental conditions as shown in Figure 7A (24 h of MG132 treatment), with the addition of a DMSO control for MG132 treatment. GFP-TDP-43-expressing cells were immunolabeled for ubiquitin. Note the ring-like pattern frequently observed surrounding (mutant) TDP-43 cytoplasmic and nuclear (arrowhead) inclusions **(B)** Representative maximum intensity Z-projections from confocal fluorescence imaging (thickness of 4 µm, in steps of 1 µm) of the same experimental conditions as shown in Figure 7C (overnight MG132 treatment), with the addition of a DMSO control. TDP-43-HA expressing human neurons were stained for ubiquitin and the neuron-specific marker MAP2. **(C)** Representative maximum intensity Z-projections from confocal fluorescence imaging (thickness of 4 µm, in steps of 1 µm) of the isogenic GFP-TDP-43 mutNLS (WT mutNLS) and

6M HEK293 lines in the same experimental conditions as shown in Figure 7A (24 h of MG132 treatment). Cells are immunolabeled for TDP-43 phosphorylated at the S409/410 epitope, which positively stains only a subset of inclusions formed in the WT mutNLS line. Note that the GFP brightness is adjusted in each condition for optimal visualization of GFP-TDP-43 localization, but the true values are higher for the WT mutNLS line. Nuclei are stained with DAPI in all images. Scale bars: 10 μm.

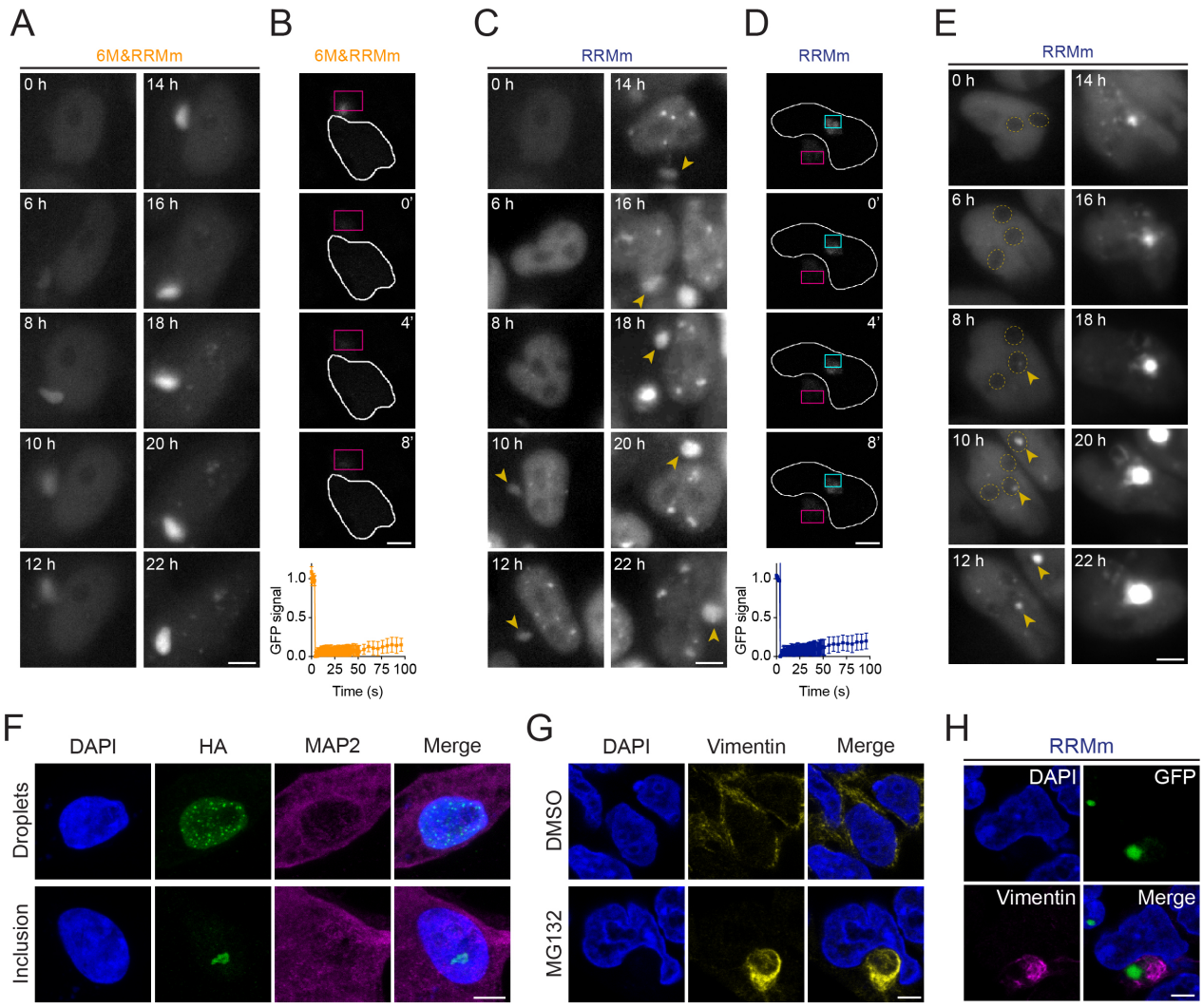

Appendix Figure S4. **Independent pathways drive TDP-43 aggregation in the nucleus and cytoplasm. (A and C)** Representative images of live widefield fluorescence microscopy over the course of the MG132 treatment depicting the formation of a cytoplasmic inclusion in the isogenic line expressing 6M&RRMm or RRMm, respectively, GFP-TDP-43 in the conditions described in Figure 7A. Numbers in images indicate the experimental time point in hours (h) of MG132 treatment. Yellow arrowheads indicate the cytoplasmic aggregate. Scale bar: 5 µm. **(B and D)** Representative fluorescent confocal microscopy images of FRAP experiments in the cytoplasmic GFP-TDP-43 6M&RRMm and RRM, respectively, aggregates originated upon MG132 treatment as described in Figure 7A. FRAP was performed in the areas highlighted in magenta. Bottom panel: Measured GFP values are expressed as a fraction of the average pre-bleach fluorescence levels. Scale bar: 5 µm. **(E)** Representative images of live widefield fluorescence microscopy over the course of the MG132 treatment depicting the presence of GFP-TDP-43 RRMm in the nucleoli of the cells under the conditions described in Figure 7A. Numbers in images indicate the experimental time point (h) of MG132 treatment. Yellow arrowheads indicate the RRMm GFP-TDP-43 accumulation in the nucleoli, which are marked by the dashed yellow lines. Scale bar: 5 µm. **(F)** Representative maximum intensity Z-projections from confocal fluorescence imaging

(thickness of 4 µm, in steps of 1 µm) of human neurons transduced with RRMm TDP-43-HA and immunolabeled for the HA tag and the neuron-specific marker MAP2 showing the presence of nuclear droplets or aggregates. Scale bar: 5 µm. **(G)** Representative confocal microscopy images of HEK293 depicting the formation of an aggresome upon treatment with MG132 for 24 h and immunolabeling for vimentin. Scale bar: 5 µm. **(H)** Confocal microscopy image of the isogenic RRMm GFP-TDP-43 line in the conditions described in Figure 7A depicting a cytoplasmic aggregate stained for vimentin. Cell nuclei are visualized with DAPI in F-H. Scale bar: 5 µm.

Cloning	Sequence (5' → 3')	Ta
TDP-43 mutagenesis F147A, F149A	GGTCATTCAAAGGGGGCTGGCGCTGTTCGTTTTACGG	72ºC
	CCGTAAAACGAACAGCGCCAGCCCCCTTTGAATGACC	
TDP-43 mutagenesis F194A	GAGAAGCAGAAAAGTGGCTGTGGGGCGCTGTACAG	72ºC
	CTGTACAGCGCCCCACAGCCACTTTTCTGCTTCTC	
TDP-43 mutagenesis F229A, F231A	CCAAGCCATTCAGGGCCGCTGCCGCTGTTACATTTGCAGATG	72ºC
	CATCTGCAAATGTAACAGCGGCAGCGGCCCTGAATGGCTTGG	
TDP-43 mutagenesis K82A, R83A, K84A	CGGCAATGGATGAGACAGATGC	57ºC
	CTGCGTTATCTTTTGGATAGTTGAC	
BamHI/XhoI-flanked TDP-43 amplification	TTAAGGATCCACCATGTCTGAATATATTCGGG	56ºC
	TTCACTCGAGCTACATTCCCCAGCCAGAAGAC	
TDP-43 mutagenesis S2C	CCATATGATGTGCGAGTATATTC	57°C
	GTATATCTCCTTCAAAAGTTAAAC	
TDP-43 mutagenesis C39S	CCCAGGCGCCTCTGGCCTGCGCT	72°C
	AACTGCGCGGTCACCGTGCTC	
TDP-43 mutagenesis C50S	GGTCAGCCAGTCCATGCGCGGTG	70°C
	GGATTACGATAGCGCAGGCC	
TDP-43 mutagenesis E14A	TGAGAACGACGCGCCGATCGAGA	66°C
	TCTTCGGTAACACGAATATACTCG	
TDP-43 mutagenesis E17A	GATTCCGAGCGCAGATGACGGTACG	70°C
	GCGATCGGCGCGTCGTTC	
TDP-43 mutagenesis E21A	GATTCCGAGCGCAGATGACGGTAC	68°C
	TCGATCGGCTCGTCGTTC	
TDP-43 mutagenesis Q34A	GGTGACCGCGGCGTTCCCAGGCG	67°C
	GTGCTCAGCAAGACCGTAC	
TDP-43 mutagenesis R52A	CCAGTGCATGGCCGGTGTCCGTC	60°C
	CTGACCGGATTACGATAG	
TDP-43 mutagenesis R55A	GGCCGGTGTCGCTCTGGTTGAGGGCATTC	67°C
	ATGCACTGGCTGACCGGA	
TDP-43 mutagenesis mutNLS	CGGCAATGGATGAGACAGATGC	57ºC
	CTGCGTTATCTTTTGGATAGTTGAC	

MBP-His6 deletion mutation	AGCGGTACCAAAATCGAAG	58°C
	CATCATATGGGTATATCTCC	

Appendix Table S1. Primers used for cloning.

Gene	Sequence (5’ → 3’)	Ref
GAPDH	AAGGTCGGAGTCAACGGATT	(Tanikawa *et al*, 2016)
	CTCCTGGAAGATGGTGATGG	
GFP	ACGTAAACGGCCACAAGTTC	(Liao *et al*, 2015)
	AAGTCGTGCTGCTTCATGTG	
TARDBP (intron 7 exclusion)	TTCATCTCATTTCAAATGTTTATGGAAG	(White *et al*, 2018)
	ATTAACTGCTATGAATTCTTTGCATTCAG	

Appendix Table S2. Primers used for qPCR.

Target	Company and reference number	WB	IF
β1	Previously published (Paganetti *et al*, 1996)	–	1:1000
c-Myc	Abcam (ab32072)	–	
Coilin	Santa Cruz Biotechnology (sc-55594)	–	1:500
GAPDH	Abcam (ab8245)	1:5000	–
GFP	Abcam (ab290)	1:5000	–
GFP (for PLA)	Abcam (ab1218)	–	1:5000
GFP	Proteintech (66002-1-Ig)	1:5000	–
G3BP	Abcam (ab56574)	-	1:400
HA	Cell Signaling Technology (3724S)	1:5000	1:500
HA	Proteintech (66006-1-Ig)	–	1:1000
HA	Biolegend (901516)	–	1:1000
HA (for PLA)	Abcam (ab256483)	–	1:6000
Histone H3	Abcam (ab1791)	1:5000	–
KPNA2	Abcam (ab70160)	1:10000	
KPNB1	Abcam (ab2811)	1:5000	
Lamin B	Proteintech (66095-1-AP)	–	1:500
MAP2	Abcam (ab5392)	–	1:1000
MAP2	Sigma (M1406)	–	1:250
p62	Proteintech (18420-I-AP)	–	1:500
PML	Santa Cruz Biotechnology (sc-377390)	–	1:50
pSC35	Santa Cruz Biotechnology (sc-53518)	–	1:500
RPA40	Santa Cruz Biotechnology (sc-374443)	–	1:50
SFPQ	Abcam (ab177149)	–	1:500
SMN	BD biosciences (610647)	–	1:200
SOD1	Enzo Life Sciences (ADI-SOD-100-F)	1:5000	
TDP-43 (3H8)	Novus Biologicals (NBP1-92695)	1:1000	1:500
TDP-43 (3H8)	Novus Biologicals (NBP1-92695PBSONLY)	–	1:6000
TDP-43 (6H6)	Proteintech (60019-2-Ig)	1:5000	–
TDP-43 (N-term)	Proteintech (10782-2-AP)	–	1:500
TDP-43 phospho-S403/404	(De Rossi *et al*, 2021)	–	1:1000

TDP-43 phospho-S409/410	CosmoBio LTD (CAC-TIP-PTD-M01)	–	1:250
TIA-1	Abcam (ab40693)	–	1:500
Ubiquitin (lys48)	Merck Millipore (05-1307)	–	1:500
Vimentin	Sigma-Aldrich (AB5733)	–	1:500
Chicken IgY, AF568-conjugated	Invitrogen (A-11041)	–	1:1000
Chicken IgY, AF647-conjugated	Invitrogen (A-32933)	–	1:1000
Human IgG, AF568-conjugated	Invitrogen (A-21090)	–	1:1000
Human IgG, AF647-conjugated	Invitrogen (A-21445)	–	1:1000
Mouse IgG, AF488-conjugated	Invitrogen (A-21202)	–	1:1000
Mouse IgG, AF568-conjugated	Invitrogen (A-10037)	–	1:1000
Mouse IgG, AF594-conjugated	Invitrogen (A-11032)	–	1:1000
Mouse IgG, AF647-conjugated	Invitrogen (A-31571)	–	1:1000
Mouse IgG, HRP-conjugated	Jackson ImmunoResearch (115-035-146)	1:5000	–
Rabbit IgG, AF488-conjugated	Invitrogen (A-21206)	–	1:1000
Rabbit IgG, AF546-conjugated	Invitrogen (A-10040)	–	1:1000
Rabbit IgG, AF647-conjugated	Invitrogen (A-31573)	–	1:1000
Rabbit IgG, HRP-conjugated	Jackson ImmunoResearch (111-035-144)	1:10000	–

Appendix Table S3. Antibodies used in this study.

References

Avendaño-Vázquez SE, Dhir A, Bembich S, Buratti E, Proudfoot N & Baralle FE (2012) Autoregulation of TDP-43 mRNA levels involves interplay between transcription, splicing, and alternative polyA site selection. *Genes Dev* 26: 1679–1684

Liao C-Y, Smet W, Brunoud G, Yoshida S, Vernoux T & Weijers D (2015) Reporters for sensitive and quantitative measurement of auxin response. *Nature methods* 12: 207–210

Paganetti PA, Lis M, Klafki H-W & Staufenbiel M (1996) Amyloid precursor protein truncated at any of the γ-secretase sites is not cleaved to β-amyloid. *Journal of Neuroscience Research* 46: 283–293

De Rossi P, Lewis AJ, Furrer J, De Vos L, Demeter T, Zbinden A, Zhong W, Wiersma VI, Scialo C, Weber J, *et al* (2021) FTLD-TDP assemblies seed neoaggregates with subtype-specific features via a prion-like cascade. *EMBO Rep* 22: e53877

Tanikawa M, Sanjiv K, Helleday T, Herr P & Mortusewicz O (2016) The spliceosome U2 snRNP factors promote genome stability through distinct mechanisms; transcription of repair factors and R-loop processing. *Oncogenesis* 5: e280–e280

White MA, Kim E, Duffy A, Adalbert R, Phillips BU, Peters OM, Stephenson J, Yang S, Massenzio F, Lin Z, *et al* (2018) TDP-43 gains function due to perturbed autoregulation in a Tardbp knock-in mouse model of ALS-FTD. *Nature neuroscience* 21: 552–563